Two methods of surface tension treatment in free surface flow simulations☆

Kirill D. Nikitin[a], Kirill M. Terekhov[b], Yuri V. Vassilevski[c],*

[a] Marchuk Institute of Numerical Mathematics, Keldysh Institute of Applied Mathematics, Russian Academy of Sciences, Moscow, Russian Federation
[b] Marchuk Institute of Numerical Mathematics, Russian Academy of Sciences, Moscow, Russian Federation
[c] Marchuk Institute of Numerical Mathematics, Russian Academy of Sciences, Moscow Institute of Physics and Technology, Sechenov University, Moscow, Russian Federation

A R T I C L E   I N F O

A B S T R A C T

We describe our approach to treatment of surface tension in free surface flow simulations on adaptive octree-type grids. The approach is based on the semi-Lagrangian method for the transport and momentum equations and the pressure projection method to enforce the incompressibility constrain. The surface tension contributes to the Dirichlet boundary condition for the pressure equation at the projection step. The treatment of surface tension is based either on accurate finite difference calculation of the mean curvature or on a curvature estimation by the implicit solution of conservative mean curvature flow problem. The first method provides almost the second order accuracy in space for surface tension forces. The second method is characterized by greater stability and essentially larger time steps. Numerical experiments illustrate the main features of the methods.

1. Introduction

Accurate numerical treatment of surface tension remains the challenge for many years since it requires accurate evaluation of the free surface curvature. The accuracy of the numerical free surface approximation depends on the accuracy of numerical treatment of both viscous incompressible fluid flow and transport of the free surface. The height function method [1] was suggested for an accurate estimation of the curvature. According to Popinet [2], although high-order curvature estimation schemes have been introduced, the overall splitting schemes, present in the literature, are still formally first-order accurate.

Our splitting method involves accurate approximations of transport, eikonal, momentum, Poisson equations, as well as the second-order method for estimation of the free surface curvature. The numerically

observed convergence rate of the resulting method demonstrates almost the second order. The momentum equation is solved with a novel combination of BDF2 (backward difference formula) and MacCormack predictor–corrector schemes. Advective terms within the scheme are treated with the semi-Lagrangian approach. Incompressibility condition is enforced with the projection method. The surface tension contributes to the Dirichlet boundary condition for the pressure equation at the projection step [3]. We consider the treatment of the surface tension by two methods: accurate finite difference calculation of the mean curvature, and curvature estimation by the implicit solution of a conservative mean curvature flow problem [4]. The first method provides almost the second order accuracy in space for surface tension forces. The second method allows us to relax considerably the time step restriction imposed by explicit and semi-implicit approaches [2].

The paper is organized as follows. Section 1 reviews the mathematical model and outlines the numerical methods used for the free surface flow modeling. Section 2 introduces two approaches for the accurate numerical treatment of the surface curvature. Section 3 presents the results of numerical experiments with an oscillating droplet driven by the surface tension.

2. Equations of free surface flow dynamics and their discretization in time

The mathematical model couples the equations of dynamics of viscous incompressible fluid, the Navier–Stokes equations for fluid velocity vector field $\mathbf{u}$ and pressure p

$$\begin{cases} \rho \left(\dfrac{\partial \mathbf{u}}{\partial t} + (\mathbf{u} \cdot \nabla)\mathbf{u} \right) - \mathrm{div}\, \left(\nu[\nabla \mathbf{u} + (\nabla \mathbf{u})^T] - p\,\mathbf{I} \right) = \mathbf{g} \\ \qquad\qquad\qquad\qquad\qquad \nabla \cdot \mathbf{u} = 0 \end{cases} \quad \text{in } \Omega(t),\ t \in (0, T], \tag{2.1}$$

and the transport equation for a Lipschitz continuous *level set* function $\phi(t, \mathbf{x})$. Given a transport field $\widetilde{\mathbf{u}}$ (extension of $\mathbf{u}$ to $\mathbb{R}^3$), the transport equation is [5]:

$$\frac{\partial \phi}{\partial t} + \widetilde{\mathbf{u}} \cdot \nabla \phi = 0 \quad \text{in } \mathbb{R}^3 \times (0, T]. \tag{2.2}$$

Zero level of function $\phi(t, \mathbf{x})$ defines the boundary $\Gamma(t)$ of the fluid domain $\Omega(t)$ where $\phi(t, \mathbf{x}) < 0$. The initial conditions $\mathbf{u}|_{t=0} = \mathbf{u}_0$ with $\nabla \cdot \mathbf{u}_0 = 0$ and $\Omega(0) = \Omega_0$ define the velocity field and the level set function $\phi(0, \mathbf{x})$, respectively. Other parameters in Eqs. (2.1) are the external force $\mathbf{g}$, the density ρ, and the kinematic viscosity ν. Eqs. (2.1) and (2.2) are coupled through the boundary conditions for (2.1) and definitions of $\widetilde{\mathbf{u}}$ and $\Omega(t)$.

For simplicity, we assume that the entire boundary $\Gamma(t)$ is a free surface, with the normal vector $\mathbf{n} = \nabla \phi / |\nabla \phi|$ and the mean curvature $\kappa = \mathrm{div}\,(\nabla \phi / |\nabla \phi|)$. The flows of our interest are governed by the capillary forces which are balanced on $\Gamma(t)$ by the normal stress $\left(\nu[\nabla \mathbf{u} + (\nabla \mathbf{u})^T] - p\,\mathbf{I} \right) \mathbf{n} = \sigma \kappa \mathbf{n}$ on $\Gamma(t)$, where σ is the surface tension parameter.

The time-stepping splits the coupled Eqs. (2.1)–(2.2) into the transport problem for ϕ, convection–diffusion problem for $\mathbf{u}$ and the Poisson problem for p. The divergence-free constrain is enforced by the standard pressure projection [6,7]. For detailed description of the fractional steps and the discretization in space we refer to [8] and [9,10], respectively. A simpler semi-discrete method was shown to conserve global momentum and angular momentum, and to satisfy an energy inequality [11]. The numerical scheme [8–10] has been developed for simulations on dynamic octree meshes refined adaptively to the free surface. For the sake of stability, the velocity components and pressure unknowns are staggered to cell faces and cell centers, respectively. Mesh adaptivity and approximation errors require additional efforts: remeshing, re-interpolation, volume correction, re-initialization. For brevity, we skip these otherwise important steps and present only steps of the scheme which are crucial in the accurate treatment of surface tension effects.

Given $\mathbf{u}^n$, ϕ^n such that $\mathrm{div}\,(\mathbf{u}^n) = 0$, $|\nabla \phi^n| = 1$, for $n = 0, 1, \dots$, we find $\mathbf{u}^{n+1}$, p^{n+1}, ϕ^{n+1} by performing the following steps:

1: Semi-Lagrangian step. Given ϕ^n and $\mathbf{u}^n$, solve (2.2) by a semi-Lagrangian method to find ϕ_d^{n+1} and set $\phi^{n+1} = \phi_d^{n+1} + \eta$ where η solves the volume conservation equation $|V(\phi_d^{n+1} + \eta) - V(\phi^n)| = 0$. Set Ω_{n+1} by $\phi^{n+1}(x) < 0$ and Γ_{n+1} by $\phi^{n+1}(x) = 0$;

2: Convection–diffusion solver. Compute the new velocity field $\widetilde{\mathbf{u}}^{n+1}$ in Ω_{n+1} by solving the convection–diffusion equation

$$(2\triangle t)^{-1}(3\widetilde{\mathbf{u}}^{n+1} - 4\mathbf{u}_d^n + \mathbf{u}_d^{n-1}) - \nu\Delta\widetilde{\mathbf{u}}^{n+1} = 0, \tag{2.3}$$

where $\mathbf{u}_d^k$ is the semi-Lagrangian solution of the transport equation for $\mathbf{u}$ on time step t^k refined by a predictor–corrector method, which allows to extend the accuracy of the second-order interpolation of the velocity field to the whole solution. For $k = n-1, n$ we define $\triangle t_k = t^{n+1} - t^k$ and for each final position of characteristic $\mathbf{x}_f$ (where a degree of freedom resides) we define the backward and forward characteristic departure points $\mathbf{x}_{d\pm}^k = \mathbf{x}_f \pm \mathbf{u}^k(\mathbf{x}_f \pm \frac{1}{2}\triangle t_k\mathbf{u}^k)\Delta t$. Then $\mathbf{u}_d^k = \hat{\mathbf{u}}^{n+1} + (\mathbf{u}^k - \hat{\mathbf{u}}^k)/2$, where

$$\hat{\mathbf{u}}^{n+1,k} = \mathbf{u}^k(\mathbf{x}_{d-}^k) - \rho^{-1}\nabla p^n \triangle t_k + \mathbf{g}\triangle t_k, \quad \hat{\mathbf{u}}^k = \hat{\mathbf{u}}^{n+1,k}(\mathbf{x}_{d+}^k) + \rho^{-1}\nabla p^n \triangle t_k - \mathbf{g}\triangle t_k.$$

3: Projection step. Project the vector field $\widetilde{\mathbf{u}}^{n+1}$ onto the discrete divergence-free subspace. Compute the new pressure p^{n+1} and velocity $\mathbf{u}^{n+1}$ from

$$-\rho^{-1}\triangle t\Delta\left(p^{n+1} - p^n\right) = 1.5\nabla\cdot\widetilde{\mathbf{u}}^{n+1} \text{ in } \Omega_{n+1}, \ \left(p^{n+1} - p^n\right) = \sigma(\kappa^{n+1} - \kappa^n) \text{ on } \Gamma_{n+1}$$

and $\mathbf{u}^{n+1} = \widetilde{\mathbf{u}}^{n+1} + \frac{2\triangle t}{3\rho}\nabla\left(p^{n+1} - p^n\right)$, respectively.

Thus the projection step implies the solution of the Poisson equation with non-homogeneous Dirichlet boundary condition based on the mean curvature to be defined on the position of interface Γ_{n+1} for given functions ϕ^{n+1} and ϕ^n. Position of Γ_{n+1} is calculated by solving the quadratic equation for ϕ^{n+1} and the curvature is interpolated linearly. The main objective of this paper is to present and study numerically two methods of the mean curvature computation at the cell centers of an octree mesh.

3. Two methods of mean curvature computation

For a level-set function $\phi \in C^2(\Omega)$, the mean curvature is computed [12] by the formula:

$$\kappa(\phi) = \left(\phi_{xx}\left(\phi_y^2 + \phi_z^2\right) + \phi_{yy}\left(\phi_x^2 + \phi_z^2\right) + \phi_{zz}\left(\phi_x^2 + \phi_y^2\right) - \right.$$
$$\left. 2\left(\phi_x\phi_y\phi_{xy} + \phi_y\phi_z\phi_{yz} + \phi_x\phi_z\phi_{xz}\right)\right)/\left(\phi_x^2 + \phi_y^2 + \phi_z^2\right)^{\frac{3}{2}}. \tag{3.1}$$

A simpler formula $\kappa(\phi) = \text{div}\,(\nabla\phi)$ assumes that ϕ has the signed distance property $|\nabla\phi| = 1$ and thus is more restrictive than (3.1).

In [9] we demonstrated how to obtain the second order approximations ϕ_{xx}^h, ϕ_{yy}^h, ϕ_{zz}^h of ϕ_{xx}, ϕ_{yy}, ϕ_{zz} at nodes of an octree cell. However, this is insufficient for the curvature estimation with (3.1), so the additional terms must be calculated.

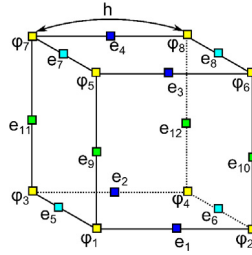First we find the third order approximations of ϕ_x at mid-edge e_1 by

$$\phi_x^h\big|_{e_1} = (\phi_2 - \phi_1)/h - h/24\left(\phi_{xx}^h\big|_2 - \phi_{xx}^h\big|_1\right),$$

and similarly for mid-edges $e_2, \ldots, e_4$ (blue) and for ϕ_y at mid-edges $e_5, \ldots, e_8$ (cyan), ϕ_z at mid-edges $e_9, \ldots, e_{12}$ (green), see Fig. 3.1.

The mixed derivative ϕ_{xy} at the cell center is approximated with the second order of accuracy by

$$\phi_{xy}^h = \left(\phi_x^h\big|_{e_2} - \phi_x^h\big|_{e_1} + \phi_x^h\big|_{e_4} - \phi_x^h\big|_{e_3}\right)/(4h) + \left(\phi_y^h\big|_{e_6} - \phi_y^h\big|_{e_5} + \phi_y^h\big|_{e_8} - \phi_y^h\big|_{e_7}\right)/(4h)$$

and similarly for ϕ_{yz}, ϕ_{xz}.

Fig. 3.1. Collocation points for ϕ^h, ϕ_x^h, ϕ_y^h and ϕ_z^h.

The second order approximation ϕ_x^h of the first derivative ϕ_x at the cell center is obtained by averaging of the central finite differences at mid-edges $e_1, \ldots, e_4$. Similarly we derive ϕ_y^h, ϕ_z^h at the cell center. The second order approximation ϕ_{xx}^h of ϕ_{xx} at the cell center is computed by averaging of the second order approximations ϕ_{xx}^h given at nodes.

As a result we have all the necessary entries for the second order evaluation of the mean curvature $\kappa(\phi^{n+1})$ at cell centers by (3.1).

The alternative method of computing the curvature $\kappa(\phi^{n+1})$ is based on the numerical solution of the unsteady mean curvature flow problem [4]

$$\frac{\partial \phi}{\partial t} - \sigma \kappa(\phi)|\nabla \phi| = 0 \quad \text{in } \mathbb{R}^3 \times (0, \triangle t]. \tag{3.2}$$

For (3.2) we apply splitting of the nonlinear spatial operator [3]:

$$\begin{aligned}
\kappa(\phi)|\nabla \phi| &= \nabla \cdot \nabla \phi - \partial_{\mathbf{n}}|\nabla \phi|, \\
\partial_{\mathbf{n}}|\nabla \phi| &= |\nabla \phi|^{-2}(\phi_{xx}\phi_x^2 + \phi_{yy}\phi_y^2 + \phi_{zz}\phi_z^2 + 2(\phi_{xy}\phi_x\phi_y + \phi_{xz}\phi_x\phi_z + \phi_{yz}\phi_y\phi_z)).
\end{aligned} \tag{3.3}$$

Note that $\partial_{\mathbf{n}}|\nabla \phi| = 0$ for ϕ satisfying $|\nabla \phi| = 1$. Therefore, the nonlinear part of $\kappa(\phi)|\nabla \phi|$ is important for functions violating the signed distance property. One time step of the operator splitting procedure is

$$(2\triangle t)^{-1}(3\widehat{\phi}^{n+1} - 4\phi^{n+1} + \phi^n) - \sigma \triangle \widehat{\phi}^{n+1} = -\sigma \partial_{\mathbf{n}}|\nabla \phi^{n+1}|, \tag{3.4}$$

which implies the solution of a linear system. We update further $\widehat{\phi}^{n+1}$ to enforce the volume conservation and the signed distance property $|\nabla \widehat{\phi}^{n+1}| = 1$.

On the other hand, function $\widehat{\phi}^{n+1}$ satisfies at least up to $O(\triangle t)$ the equation

$$(2\triangle t)^{-1}(3\widehat{\phi}^{n+1} - 4\phi^{n+1} + \phi^n) - \sigma \kappa(\widehat{\phi}^{n+1})|\nabla \widehat{\phi}^{n+1}| = O(\triangle t)$$

which implies due to $|\nabla \widehat{\phi}^{n+1}| = 1$

$$\sigma \kappa(\widehat{\phi}^{n+1}) = (2\triangle t)^{-1}(3\widehat{\phi}^{n+1} - 4\phi^{n+1} + \phi^n) + O(\triangle t). \tag{3.5}$$

As the alternative to (3.1), we use (3.5) for evaluation of surface tension forces $\sigma \kappa(\phi^{n+1})$. We note that both methods define mean curvature $\kappa(\phi^{n+1})$ in all cells of the mesh, not only on cells intersecting Γ_{n+1}.

4. Numerical test

For experimental study of the mean curvature evaluations we consider a free droplet ($\mathbf{g} = 0$) whose oscillations are driven only by surface tension forces. The problem is challenging for the surface tension force approximation since it requires computation of an accurate and smooth curvature field. This is the benchmark test for free surface and two-phase fluid flow solvers, see, e.g., [13–17].

Table 4.1
Convergence (in space–time) to the reference value T_{ref}, two methods of curvature calculation.

Mesh $10/(3h_{\min})$	Time step $\triangle t$	Period T	Period error $|T - T_{\mathrm{ref}}|$	Ratio	Period T	Period error $|T - T_{\mathrm{ref}}|$	Ratio
		Finite differences (3.1)			Mean curvature (3.5)		
32	0.0134	2.44616	0.22476	–	2.34712	0.12572	–
64	0.00474	2.28401	0.06261	1.84392	2.24766	0.02626	2.259
128	0.00168	2.24034	0.01894	1.72495	2.20632	0.01508	0.8002

Table 4.2
Convergence (in time) to the reference value T_{ref}, mean curvature estimation by (3.5).

Time step $\triangle t$	Period T	Period error $|T - T_{\mathrm{ref}}|$	Ratio
1/10	2.9	0.6786	–
1/20	2.55	0.3286	1.0462
1/40	2.35	0.1286	1.3534
1/80	2.275	0.0536	1.2626

At time $t = 0$, the fluid is assumed to be at rest and $\Omega(0)$ is a perturbation of a sphere: in spherical coordinates (r, θ, φ) $\Gamma(0)$ is given by $r = r_0(1 + \epsilon S_2(\pi/2 - \theta))$, where S_2 is the second spherical harmonic. Since the mean curvature of $\Gamma(0)$ is not constant, the non-uniform surface force causes droplet motion. The oscillatory motion demonstrates the continuous transition between the kinetic and free surface energy. The fluid viscosity results in the exponential decay of the oscillations due to the dissipation [11]. According to [18,19], the period and the damping factor for oscillations are $T_{\mathrm{ref}} = 2\pi\sqrt{\rho r_0^3/(8\sigma)}$ and $\delta_{\mathrm{ref}} = r_0^2/(5\nu)$, given that the flow is irrotational. In a number of works [13–16,19–21], one compares these values to the values recovered in the numerical experiment. The numerical error for the period is assumed to represent the error for surface tension forces, whereas the damping factor can be used in estimation of the numerical viscosity.

We set $r_0 = 1$, $\sigma = 1$, $\epsilon = 0.3$, $\nu = 0$, $\rho = 1$ which imply $T_{\mathrm{ref}} = 2.2214$ and $\delta_{\mathrm{ref}} = \infty$ (numerical damping is due to the numerical viscosity only). The octree mesh for the cube $[0, 10/3]^3$ is refined dynamically towards $\Gamma(t)$ with minimal mesh size $h_{\min} = 10/(3 \cdot 2^k)$, $k = 5, 6, 7, 8$, the largest mesh size is $h_{\max} = 10/(3 \cdot 2^4)$ in all the cases. Table 4.1 shows the computed period of the oscillations for computation of the curvature by the finite differences (3.1) and the mean curvature flow (3.5) on different meshes. In order to ensure the stability, we used the time step $\triangle t \leq C\sqrt{\frac{\rho}{2\pi\sigma}}\triangle x^{3/2}$ [2]. One observes almost the second order convergence rate for $|T - T_{\mathrm{ref}}|$ for the explicit method of calculation and considerable reduction in convergence rate for the implicit method. A possible reason for deterioration of the convergence rate is higher numerical dispersion and dissipation, see comments to Fig. 4.1 (right).

Table 4.2 presents the computed period of the oscillations for the curvature computation by the transport equation on the mesh with $h_{\min} = 10/(3 \cdot 2^6)$. Since the method has no practical restrictions on the time step, we vary $\triangle t$ from 0.1 to 1/80. One clearly observes the first order of convergence in time. Table 4.3 demonstrates the convergence of the period T for the mean curvature calculation by the mean curvature flow on different meshes. Fig. 4.1 (left) compares the dynamics of the droplet diameter along z axis for two simulations on the mesh with $h_{\min} = 10/(3 \cdot 2^6)$: finite differences calculation of the curvature with $\triangle t = 0.00474$ versus the curvature computed implicitly by the transport equation, $\triangle t = 0.1$. The large time step produces the dispersion error and high numerical viscosity: the oscillations are damped faster and their period is larger.

For equal small time steps both methods provide close results, but oscillations damp a bit faster with the implicit method, see Fig. 4.1 (right) indicating its higher numerical dispersion and dissipation. If we account presence of very large cells $h_{\max} = 10/(3 \cdot 2^4)$, we conclude that both methods demonstrate low numerical dissipation.

Table 4.3
Convergence (in space–time) to the reference value T_{ref}, mean curvature estimation by (3.5).

Mesh $10/(3h_{\min})$	Time step $\triangle t$	Period T	Period error $|T - T_{\mathrm{ref}}|$	Ratio
32	1/50	2.38	0.1586	–
64	1/100	2.3	0.0786	1.0182
128	1/200	2.255	0.0336	1.2261
256	1/400	2.2325	0.0111	1.5979
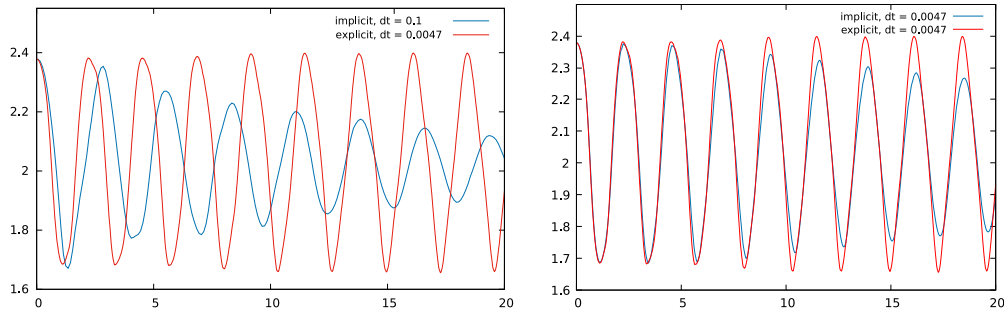
Fig. 4.1. Droplet diameter along z axis: finite difference calculation of curvature with $\triangle t = 0.00474$ vs. curvature computed implicitly with $\triangle t = 0.1$ (left); finite difference calculation of curvature with $\triangle t = 0.00474$ vs. curvature computed implicitly with $\triangle t = 0.00474$.

References

[1] S. Popinet, An accurate adaptive solver for surface-tension-driven interfacial flows, J. Comput. Phys. 228 (16) (2009) 5838–5866.
[2] S. Popinet, Numerical models of surface tension, Annu. Rev. Fluid Mech. 50 (1) (2018) 49–75.
[3] P. Smereka, Semi-implicit level set methods for curvature and surface diffusion motion, J. Sci. Comput. 19 (1) (2003) 439–456.
[4] M. Sussman, M. Ohta, A stable and efficient method for treating surface tension in incompressible two-phase flow, SIAM J. Sci. Comput. 31 (4) (2009) 2447–2471.
[5] S. Osher, R. Fedkiw, Level Set Methods and Dynamic Implicit Surfaces, Springer-Verlag, 2002.
[6] A. Chorin, Numerical solution of the Navier-Stokes equations, Math. Comp. 22 (1968) 745–762.
[7] O. Pironneau, On the transport-diffusion algorithm and its applications to the Navier–Stokes equations, Numer. Math. 28 (1982) 309–332.
[8] K. Nikitin, M. Olshanskii, K. Terekhov, Y. Vassilevski, A splitting method for free surface flows over partially submerged obstacles, Russian J. Numer. Anal. Math. Modelling 33 (2) (2018) 95–110.
[9] K. Terekhov, K. Nikitin, M. Olshanskii, Y. Vassilevski, A semi-Lagrangian method on dynamically adapted octree meshes, Russian J. Numer. Anal. Math. Modelling 30 (6) (2015) 363–380.
[10] K. Nikitin, M. Olshanskii, K. Terekhov, Y. Vassilevski, R. Yanbarisov, An adaptive numerical method for free surface flows passing rigidly mounted obstacles, Comput. & Fluids 148 (2017) 56–69.
[11] K. Nikitin, M. Olshanskii, K. Terekhov, Y. Vassilevski, A splitting method for numerical simulation of free surface flows of incompressible fluids with surface tension, Comput. Methods Appl. Math. 15 (1) (2015) 59–78.
[12] G. Buttazzo, A. Visintin (Eds.), Motion by mean curvature and related topics, in: Proceedings of the International Conference at Trento, Walter de Gruyter, New York, 1994.
[13] E. Bänsch, Finite element discretization of the Navier–Stokes equations with a free capillary surface, Numer. Math. 88 (2) (2001) 203–235.
[14] M.M. Francois, S.J. Cummins, E.D. Dendy, D.B. Kothe, J.M. Sicilian, M.W. Williams, A balanced-force algorithm for continuous and sharp interfacial surface tension models within a volume tracking framework, J. Comput. Phys. 213 (1) (2006) 141–173.
[15] S. Ganesan, L. Tobiska, An accurate finite element scheme with moving meshes for computing 3D-axisymmetric interface flows, Internat. J. Numer. Methods Fluids 57 (2) (2008) 119–138.
[16] S. Ganesan, L. Tobiska, A coupled arbitrary Lagrangian–Eulerian and Lagrangian method for computation of free surface flows with insoluble surfactants, J. Comput. Phys. 228 (8) (2009) 2859–2873.
[17] S. Quan, D.P. Schmidt, A moving mesh interface tracking method for 3D incompressible two-phase flows, J. Comput. Phys. 221 (2) (2007) 761–780.
[18] H. Lamb, Hydrodynamics, Dover Publications, New York, 1945 pp. 475, 640.
[19] W. Cheng, M. Olshanskii, Finite stopping times for freely oscillating drop of a yield stress fluid, J. Non-Newton. Fluid Mech. 239 (2017) 73–84.

[20] D. Torres, J. Brackbill, The point-set method: front-tracking without connectivity, J. Comput. Phys. 165 (2) (2000) 620–644.
[21] D. Enright, D. Nguyen, F. Gibou, R. Fedkiw, Using the particle level set method and a second order accurate pressure boundary condition for free surface flows, in: ASME/JSME 2003 4th Joint Fluids Summer Engineering Conference, American Society of Mechanical Engineers, 2003, pp. 337–342.